https://doi.org/10.48048/tis.2022.5763

Synthesis and Characterization of Zinc Vanadate Nanostructures for Supercapacitor Applications

Lakshmana Naik Ramavathu[*] and Balanarsaiah Tumma

JNTU College of Engineering, Ananthapuramu, Andhra Pradesh, India

([*]Corresponding author's e-mail: lakshman2027@gmail.com)

Received: 1 August 2021, Revised: 21 September 2021, Accepted: 30 September 2021

Abstract

A simple hydrothermal approach was used to successfully produce nanostructured Zinc vanadate ($Zn_3V_2O_8$), which was calcined at 450 ℃. The structural, optical and surface morphological features of calcined $Zn_3V_2O_8$ nanoparticles were investigated using a variety of analytical techniques. The produced $Zn_3V_2O_8$ nanoparticles had an orthorhombic crystalline structure, with an average crystallite size of 35.14 nm, according to the X-ray diffraction pattern (XRD). Transmission electron microscopy (TEM) analysis evaluated the spherical shaped $Zn_3V_2O_8$ nanoparticles. The calcined catalyst was characterized by Fourier Transform-Infrared spectroscopy (FT-IR) analysis to analyse bonding interactions between the metal fragments within the composites**.** The nanoparticles obtained from hydrothermal synthesis were of size 37.2 nm, and the zeta-potential of nanoparticles was found to be −25.4 mV, indicating excellent dispersion and stability. The spectrophotometer was used to analyse the UV-Vis diffuse reflectance spectra (DRS). Cyclic voltammetry and electrochemical impedance spectroscopy were used to study the electrochemical behavior of $Zn_3V_2O_8$ nanostructures. The specific capacitance value of the synthesized nanoparticles was 248.5 Fg^{-1}. The active composite material was exploited as an electrode for the Supercapacitor application, and it revealed that synthesized $Zn_3V_2O_8$ nanoparticles might lead to a possible application for future energy storage technologies.

Keywords: Zinc metavanadate, Hydrothermal treatment, Specific capacitance, Supercapacitor

Introduction

Supercapacitors, unlike batteries, store energy as a charge on the electrode surface or subsurface layer rather than in the bulk material [1]. Because of these distinguishing characteristics, the supercapacitor is one of the most promising energy storage devices [2]. Because of their better performance, energy storage methods based on electrochemical reactions have gained popularity [3]. Supercapacitors are an electrochemical energy storage device that significantly impacts the efficiency of power devices and is the most practical alternative for automobiles [4]. Supercapacitors have a greater power density than conventional capacitors and batteries, good cycle stability, higher rate capacity and longer life [5,6]. Electric double layer capacitors (EDLCs), hybrid capacitors, and pseudocapacitors are the 3 types of energy storage mechanisms that are influenced by the charges stored at the electrode and electrolyte interface [7]. Second, pseudocapacitors, powered by charge transfer between electrode/electrolyte interfaces, resulting in a quicker redox process [8]. The use of redox reactions of electrolyte ions in electrode materials is at the heart of a supercapacitors demand for high power density [9]. Electrochemical devices, particularly supercapacitors, employ transition metal oxides (ZnO, RuO_2, NiO, MnO_2, Co_3O_4, CuO and Fe_2O_3), carbon-based materials (graphene, carbon spheres and carbon nanotubes), and conducting polymers as electrode materials [10,11].

On the other hand, mixed transition metal oxides would be a step forward for quick charge-discharge rates and longer usage lifetime since they entail faster Faradic reactions and give higher specific capacitance values [12,13]. Transition metal oxides have a 3-fold higher theoretical specific capacity than commercially available graphite [14]. In this perspective, vanadium pentoxide (V_2O_5), with its various oxidation states, has attracted a lot of scientific attention [15,17]. In recent years, many research groups have used metal vanadates (Mn, Zn, Cu, Ni, Co, Fe, etc.) as electrodes, and considerable effort has been made to synthesize various kinds of nanocomposite capacitive materials as mixed metal oxides [18-20]. V_2O_5 layered structure allows for more interlayer locations for various guest species to intercalate [21].

Furthermore, during the electrochemical process of forming amorphous VOx matrixes, aggregation of various metal species is significantly reduced [22]. Because of their low cost, high specific capacity, environmental suitability, and ease of availability, zinc vanadium oxides have attracted particular interest among the different mixed tri-metal vanadate [23,24].

Many vanadium oxide nanostructures, such as nanorods, nanobelts and nanowires, have been explored for use as electrode materials [25]. Vanadium nanoparticles enable the use of vanadium oxide as a metal cation to boost electrochemical productivity. They also offer numerous advantages, such as being environmentally friendly, having high operational stability, having a simple preparation procedure, and being inexpensive [26]. They have a reduced internal resistance, which is helped by more excellent ionic conductivity and protons' rapid mobility, making them a desirable alternative [27]. The produced $Zn_3V_2O_8$ yielded findings that were equivalent to those obtained before. The electrochemical behaviour of a nickel-based metal oxide compound was investigated by hydrothermal method, and the material's energy storage capacity (specific capacitance) was determined to be 193.5 Fg^{-1} with a high reversibility [28]. Furthermore, zinc vanadate nanoparticles with a specific capacitance of 312 Fg^{-1} were produced using a simple co-precipitation process and calcined at 600 ℃ [29]. Surprisingly, increasing the operating voltage of electrolytes can enhance the supercapacitor's total functioning potential. Currently, ternary metal oxides pseudo capacitors showed advanced specific capacitance values because of ternary metal oxide's triple oxide states, outstanding electrical conduction, and exemplary electrochemical behaviour.

The present work reports the preparation of $Zn_3V_2O_8$ nanostructures by the simple hydrothermal route. The prepared $Zn_3V_2O_8$ were characterized for crystallinity, phase, structural and morphological properties using advanced analytical tools. A detailed study of the super capacitive property of the electrode material has been performed in 0.1 M HCl using CV and EIS techniques. This work depicts the intention to utilize $Zn_3V_2O_8$ based electrochemical studies for a broad spectrum of energy to promote environmentally friendly, sustainable, and cleaner technology for a brighter world.

Experimental section

Materials

Materials used for the preparation of $Zn_3V_2O_8$ were of analytical reagent (A.R.) grade purchased from Sigma Aldrich, Germany they are Zinc acetate dihydrate $Zn(CH_3CO_2)_2{\cdot}2H_2O$, Ammonium metavanadate (NH_4VO_3, ≥ 99.0 %), N-methyl-2-pyrrolidone (C_5H_9NO), urea (CH_4N_2O), ethanol (C_2H_5OH) and double distilled water (H_2O, lab-made).

Synthesis of zinc vanadate nanoparticles

A simple hydrothermal process was used to make $Zn_3V_2O_8$ nanomaterial, in a typical synthesis, 87.5 mL of N-Methyl-2-Pyrrolidone was added to a solution containing 1.323 g of NH_4VO_3 (ammonium metavanadate) with steady magnetic stirring of 300 rpm for 1 h (Solution A). 8.450 g of urea was added to solution A with steady stirring. In 250 mL of water, 3.76 g of zinc acetate were added (solution B). Then, with constant stirring of 340 rpm, solution B was gently combined with solution A. Finally, the blended solution was diluted to 350 mL, transferred to a Teflon-lined autoclave, and heat-treated for 36 h at 160 ℃. After cooling to ambient temperature, the powder in the autoclave was centrifuged, rinsed with deionized water, washed again with 100 % ethanol, and dried at 80 ℃ for 12 h. To obtain highly crystalline powders, the dry material was calcined in air for 3 h at 450 ℃ with a heating rate of 2 ℃/min. The calcined sample is used for further characterization.

Sample characterization

A diffractometer (CoK, PANalytical, X'Pert, data converted to CuK) was used to record X-ray powder diffraction (XRD) patterns. A JEOL2010 transmission electron microscopy was used to take the images. To analyse the characteristics of synthesized nanoparticles, U.V - Visible absorption spectra were recorded using a UV 1,800 spectrophotometer. A spectrometer was used to examine functional groups of the prepared sample using a Fourier transform infrared spectrometer (FT-IR) within the range of 4,000 to 400 cm^{-1} using the KBr pellet technique.

Results and discussion

Morphological and structural analysis of $Zn_3V_2O_8$ nanomaterials

XRD pattern of hydrothermally produced crystalline $Zn_3V_2O_8$ nanomaterial (**Figure 1**). The quantitative investigation was carried out with the software bundle, version 3.0, High Score Plus. The peaks locations at 2θ are 15.1, 23.2, 26.5, 29.4, 31.1, 34.9, 36.07, 43.27, 57.9 and 62.9 can be readily

indexed as (020), (021), (022), (131), (040), (122), (023), (240), (025) and (442), correspondingly, complies with the standard pattern as mentioned in JCPDS card no. 34-0378 [28]. The high-intensity peaks suggest that the synthesized nanoparticles were strongly crystalline in nature, and all of the peaks closely matched JCPDS number 34-0378. Space group-Cmca without any impurity with a = 6.088 Å, b = 11.489 Å, c = 8.280 Å Density: ρ = 4.88 g·cm^{-3}. Orthorhombic (space group-Cmca) lattices are created by extending a cubic lattice along 2 orthogonal pairs by 2 distinct factors, a/b (0.529), b/c= 1.387 and c/a = 1.36, resulting in a rectangular prism with variable lattice parameters (a, b and c), as shown in **Table 1**.

Table 1 Lattice parameters of $Zn_3V_2O_8$ nano structure.

Lattice parameters								
a (Å)	**b (Å)**	**c (Å)**	**α = β = γ**	**a/b**	**b/c**	**c/a**	**V (Å^3)**	**D (nm) For plane (122)**
6.088	11.489	8.280	90^o	0.52	1.38	1.38	555.52	11.8

Space group: Cmca
Structure: Orthorhombic

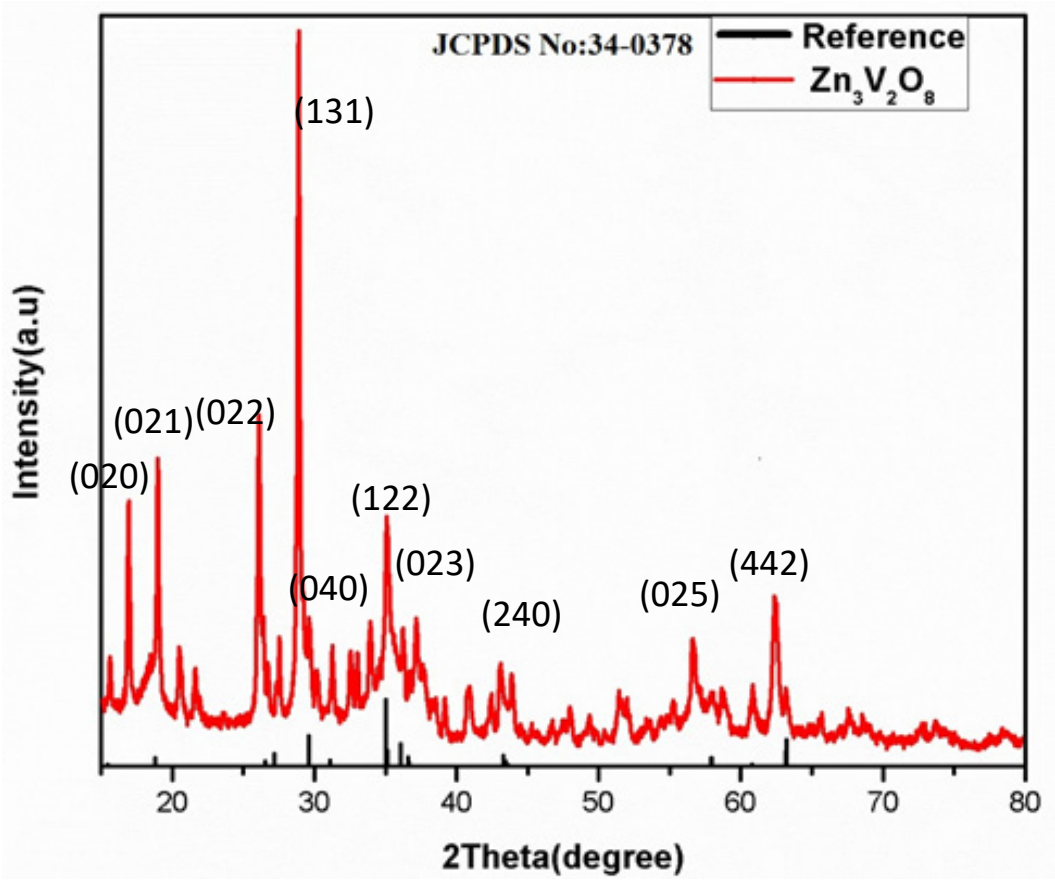

Figure 1 XRD pattern of $Zn_3V_2O_8$ nanoparticles.

Using Scherrer's Eq. (1) [30],

$$D = \frac{k\lambda}{\beta\cos\theta} \quad (1)$$

The mean crystallite size of synthesized nanoparticles was deducted to be ~ 35.14 nm. D is the average crystallite size, for orthorhombic structure K is the shape factor or Scherrer constant, which has a constant value of 0.89, θ is the Bragg's diffraction angle, λ (1.540 Å) is the wavelength of X-ray source, and β is full width at half maximum (FWHM).

HR-TEM investigations with different magnifications were used to study morphology of the surface and the structure of synthesized $Zn_3V_2O_8$ nanoparticles, as shown in **Figure 2**. The TEM images of $Zn_3V_2O_8$ nanoparticles in **Figure 2** (a - f) indicate that the produced nanoparticles had a spherical morphology and varied nanostructured sizes. An assembly of interlinked platelets developing in all directions could be responsible for the growth of a spherical-shaped structure. With a uniform distribution, the size ranges significantly between 5 and 50 nm. Furthermore, the nanoparticles of $Zn_3V_2O_8$ appear to agglomerate together, indicating a high surface charge and activity.

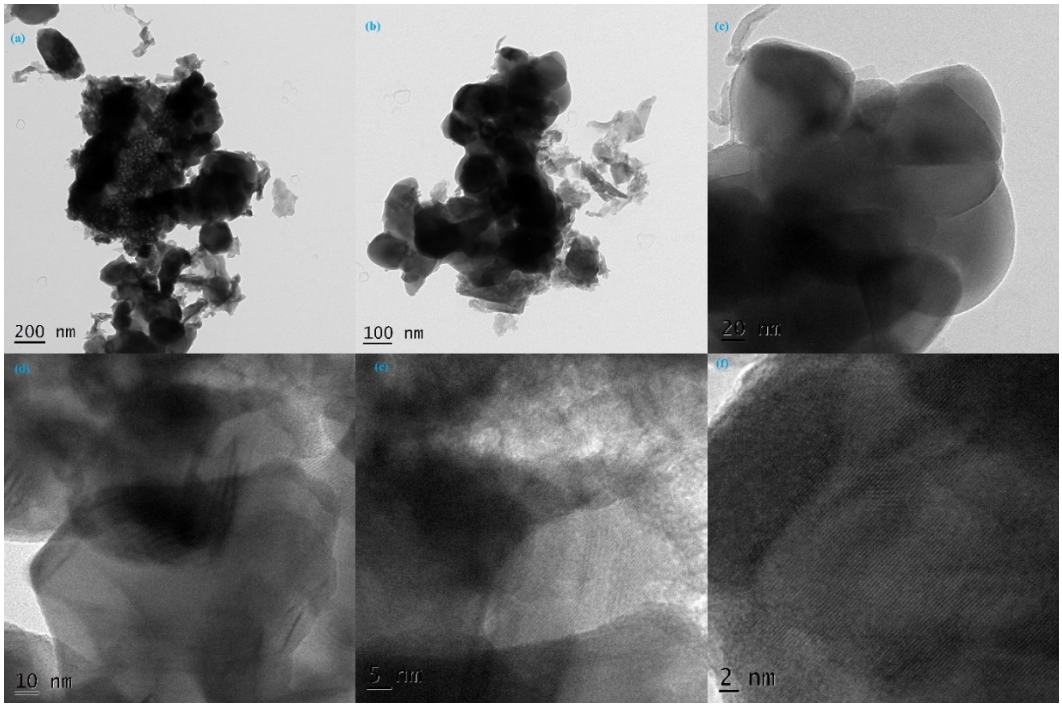

Figure 2 TEM micrographs of $Zn_3V_2O_8$ nanoparticles at different magnifications (a - f) 200, 100, 20, 10, 5 and 2 nm, respectively.

FT-IR

Figure 3(a) depicts the characteristic FTIR spectrum of $Zn_3V_2O_8$ nanoparticles. The spectra exhibit a broad absorption peak in the 3,600 - 3,000 cm^{-1} wavenumber band, to which the hydroxyl groups and water molecules can be attributed. Peak appearances at 467 and 930 cm^{-1} were assigned to the V-O-Zn band and VO_4^{3-} vibrations, respectively. Bands having wavenumbers between 925 and 935 cm^{-1} are ascribed to vanadate stretching modes (V-O). V-O-V stretching was ascribed to bands between 650 and 780 cm^{-1} because of metal group V-O-V stretching in tetrahedral vibration of VO_4. Because of the bonds shared by corner atoms of the tetrahedral structure (VO_4), the vibration band in the range of 770 - 650 cm^{-1} is attributed to V = O [31]. This band, part of the extended mode of Zn-O, Zn -O-V, and Zn -O-Zn type bonds, has been examined in the FTIR band around 467 cm^{-1}. The absence of extra peaks in the FTIR spectrum demonstrated that the processed material was highly pure. However, the presence of peaks in the visible spectrum suggested that the compound contained only metal oxide vanadate, which was perfectly according to XRD.

Figure 3(b) depicts the energy gap spectrum, and **Figure 3(b)** showing the diffused reflectance spectrum of $Zn_3V_2O_8$ nanostructures. Kubelka-Munk's (K.M.) equation (Eqs. (2) - (3)) was used to calculate the energy bandgap value and was found to be 5.475 eV. Diffuse reflectance was established to enable materials analysis such as powders and papers in their well-ordered state. The mutual distinguishing of these constituents is their internal inhomogeneities. The propagation of light through

such inhomogeneous media changes meaningfully from the propagation of light in a homogeneous material since the light scatters off points in its path. Thus, the key to the theoretical description of diffuse reflection lies in describing the propagation of light through inhomogeneous materials. However, only approximate descriptions exist. The most widely used model for diffuse reflection is the one put forward by Kubelka and Munk.

$$F(R) = \frac{(1-R)^2}{2R} \quad (2)$$

$$F(R)hv = A(hv - Eg)^n \quad (3)$$

F(R) is the absolute function reflection (R), also called Kubelka-Munk function, A and hv are constant, and energy of the photon for n = ½, indirectly allowed transition and n = 2, directly allowed transition [32,33].

As shown in **Figure 4(a)**, the particle size distribution of $Zn_3V_2O_8$ was further confirmed by DLS. According to the DLS analysis, the range of $Zn_3V_2O_8$ was observed to be 14.5 - 300 nm in size, indicating a broad size distribution of particles with an average particle size of 37.2 nm. $Zn_3V_2O_8$ nanoparticles have a polydispersity index (P.I.) of 3.492.

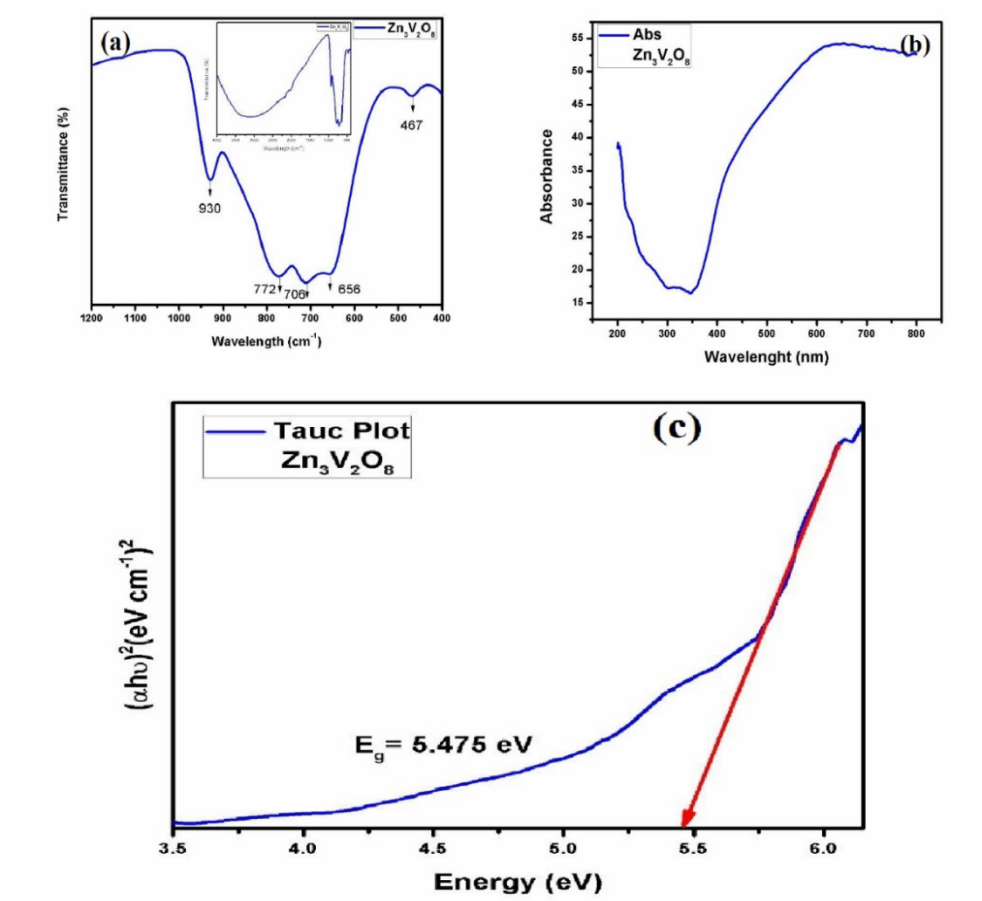

Figure 3 (a) FTIR spectroscopy of $Zn_3V_2O_8$, (b) UV-Visible diffuse reflectance spectra, (c) DRS spectra and Kubelka-Munk function vs energy gap of $Zn_3V_2O_8$.

Dynamic light scattering analysis was used to evaluate the zeta potential value of produced nanoparticles. The zeta potential of the calcined nanomaterial $Zn_3V_2O_8$ is an essential component in determining its durability. In this work, the Zeta potential of $Zn_3V_2O_8$ was discovered to be −25.4 mV, as shown in **Figure 4(b)**. Due to negative-negative repulsion, a high negative zeta potential suggests that $Zn_3V_2O_8$ is long-term stable without agglomeration and supports strong colloidal nature and excellent

dispersion of produced $Zn_3V_2O_8$. Nanomaterials must have a high level of stability in order to be used in an energy storage device.

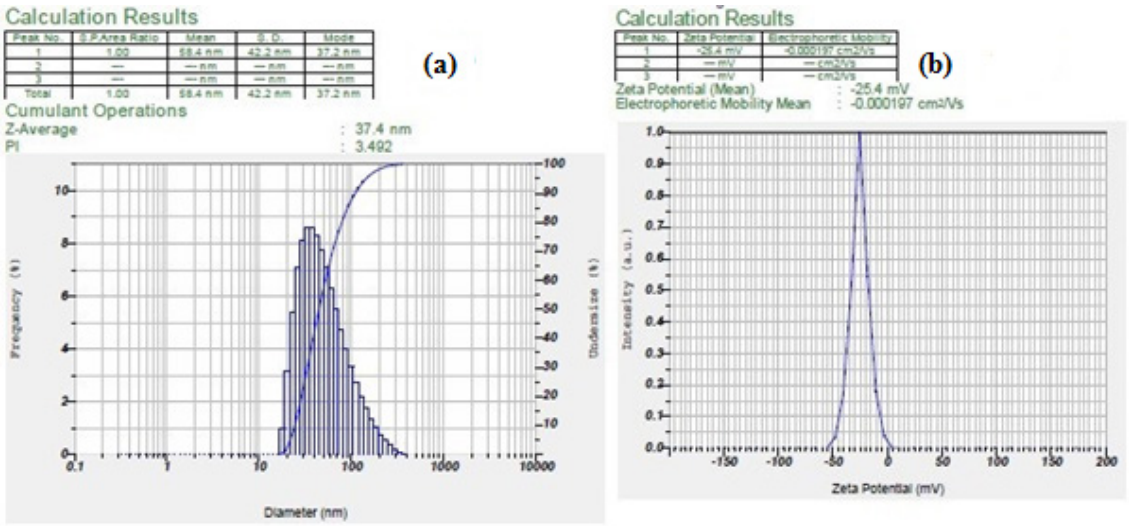

Figure 4 (a) Analysis of average particle size, particle size distribution and polydispersity index of $Zn_3V_2O_8$, (b) Zeta potential of $Zn_3V_2O_8$ nanoparticles.

Electrochemical measurements

Electrochemical impedance spectroscopic (ESI) studies were done using cyclic voltammetry (CV) and A.C. impedance using a 3-electrode cell in 0.1 M (molar) HCl (hydrochloric acid) at room temperature (R.T.). The Cyclic Voltammogram graphs show the efficiency of charge and electrode reaction reversibility. $Zn_3V_2O_8$ active carbon paste electrode shows (**Figure 5**) CV plots at scan rates vary from 0.010 to 0.050 V/s in 0.1 M HCl, respectively. There is a variation in the CV properties due to the scan rates, which can be observed in plots. As the scan rate increases, there is a noticeable increase in the peak current (IP) responsible for both oxidation and reduction, which says there is a quick movement of the electrons in the working electrode interface and mainly at the electrolyte. Electrochemical Impedance studies were performed on an Electrochemical Analyzer (CH Instruments model-608E) having a 3-electrode system.

The electrode's CV measurements show a pseudocapacitive feature to attain high power density and large capacitance values. As a result of faradaic interactions of the substance (electrode) with ions of the electrolyte, the CV reveals a pair of reversible redox maxima (**Figure 5**) [34]. The electrolyte's ionic conductivity is essential in determining an electrode's capacitance, and these ions have an ionic size equal to or less than the pore size of the user working electrode. As a result, hydrated ions diameters have a significant impact on ionic conductivity and electrode-specific capacitance.

Later this was calculated using relation (4) [35,36].

$$C_{sp} = \frac{S}{mk\Delta V} \quad (4)$$

where, S, m, k, and ΔV indicate the area under the CV curve, weight of active material used in the electrode, voltage window, or the change in the voltage and rate of scanning, respectively. The area under the CV curve for any electrode, which gives the overall charge (Q) stored, is directly related to specific capacitance. From this, it can be said that a large area in the electrode is directly proportional to the generation of a large capacitance at a particular mass of loaded electrode material (substance) and a known potential window. The electrode's specific capacitance value in 0.1 M HCl was estimated using Eq. (1) as 248.5 Fg^{-1}.

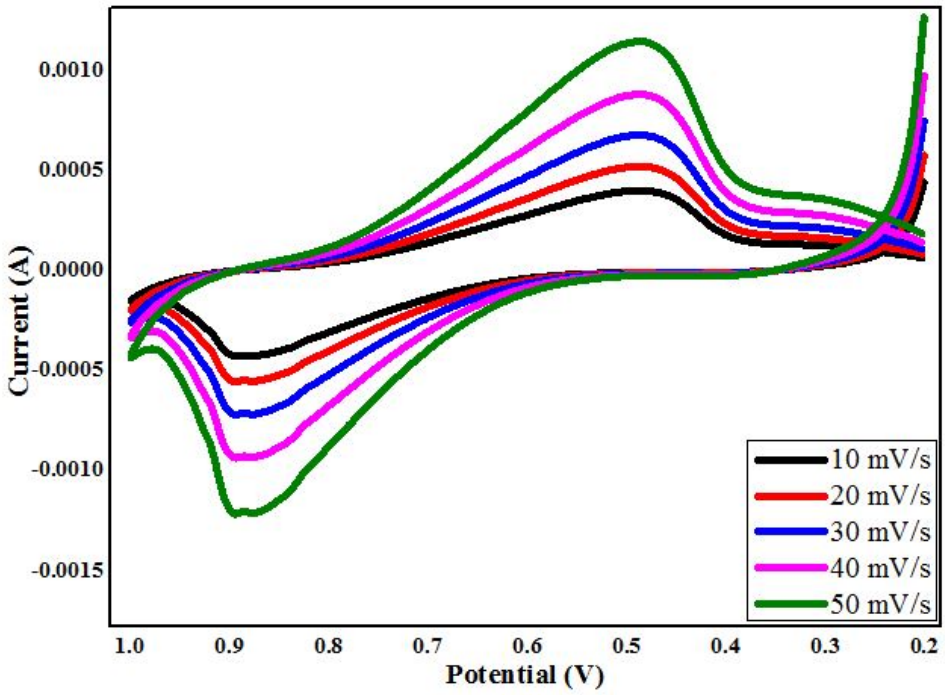

Figure 5 Cyclic Voltammogram of $Zn_3V_2O_8$ at different scan rates.

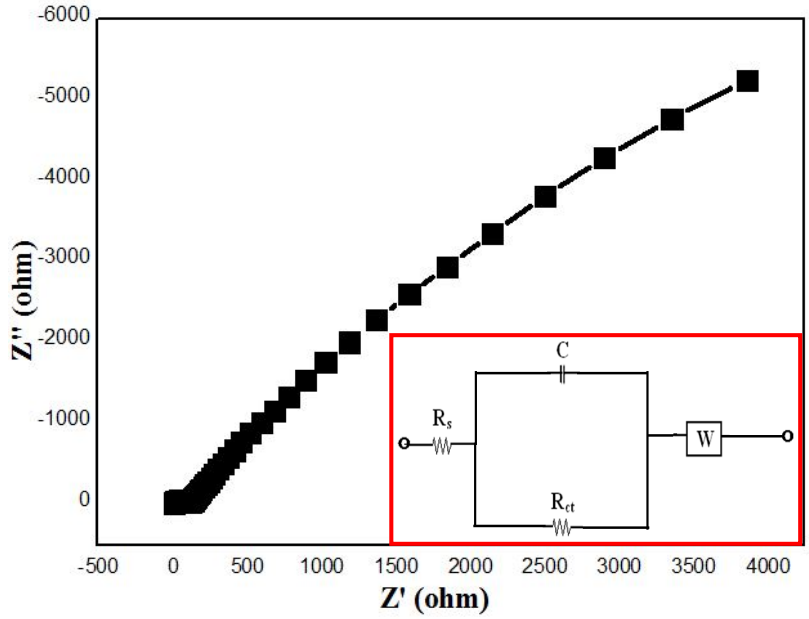

Figure 6 Nyquist plot of $Zn_3V_2O_8$ electrode (Inset-equivalent circuit).

The charge transfer characteristics of the $Zn_3V_2O_8$ electrode were studied by performing electrochemical impedance spectra (EIS) in 0.1 N HCl electrolyte in the frequency range 1 Hz^{-1} MHz at 5 mV amplitude (**Figure 6**). The resistance at the interface of the active electrode and electrolyte was determined from the semicircles of Nyquist plots. The impedance spectrum of an electrode displayed a lowered arc with a smaller diameter in the region of high frequency, revealing the low charge transfer resistance (Rct) and high capacitance (C) of the electrode.

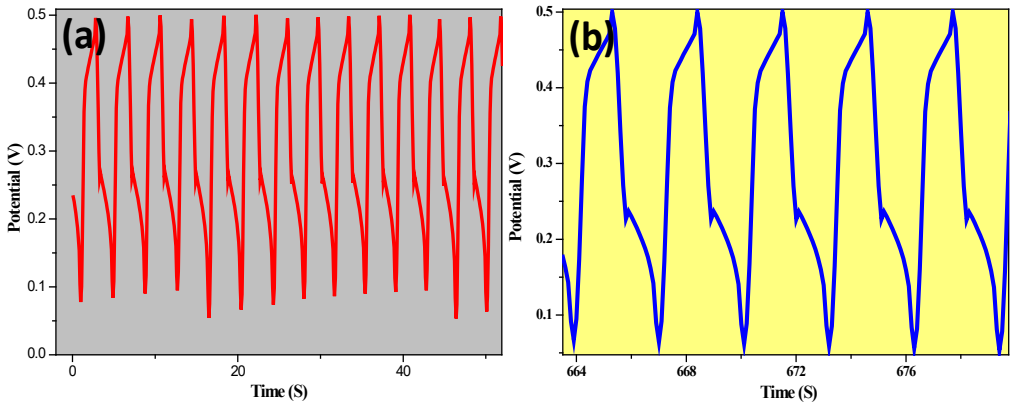

Figure 7 Galvanostatic charge-discharge curves of $Zn_3V_2O_8$ electrode: (a) 1st 10 cycles and (b) last 5 cycles of 100 cycles.

Figures 7(a) and **7(b)** shows the GCD profile of $Zn_3V_2O_8$ NPs at 5 A/g current density in 0.1 M HCl solution. The GCD profile illustrates symmetric charging and discharging curves. Owing to the resistance factor between the electrode and electrolyte interface a small IR drop at the point of conversion from charging to discharging can be noticed. The pseudo capacitance nature of the electrode is responsible for the coulomb efficiency and high reversibility of faradic ion kinetics, which is clear from the symmetric GCD profile of the charging and discharging studies. The specific capacitance $Zn_3V_2O_8$ NPs from the GCD curves can be estimated using the following expression:

$$C_s = \frac{i\,\Delta t}{m\Delta v} \tag{5}$$

where, i is the applied current, Δt is the discharging time, m is the mass of the active material loaded onto the substrate, and Δv is the potential window. The GCD curve of $Zn_3V_2O_8$ NPs exhibits outstanding coulomb efficiency after long cycles with retention in the pattern of the curves even after 100 cycles (**Figure 7(b)**).

Conclusions

A simple hydrothermal technique was used to synthesize unique zinc Metavanadate nanoparticles successfully. To improve the prepared sample's crystallinity, it was calcined at 450 °C. XRD and FTIR techniques examined the pure orthorhombic structure, cell properties, and functional group of $Zn_3V_2O_8$ nanoparticles. HR-TEM images revealed the shape of $Zn_3V_2O_8$ nanoparticles and proved the lattice resolution, which matched the XRD results. The produced $Zn_3V_2O_8$ has a bandgap of 5.475 eV, according to the study. The formation and stability of nanoparticles are confirmed by particle size and Zeta potential. Furthermore, the faradaic pseudo capacitive character of $Zn_3V_2O_8$ nanoparticles demonstrates exemplary electrochemical behaviour. The maximum significant specific capacitance value was 248.5 Fg^{-1}. The agglomerated nanostructure with outstanding electrochemical performance was perfect for Supercapacitor application due to its unusual redox activity.

References

[1] D Yang. *Application of nanocomposites for supercapacitors: Characteristics and properties. In*: F Ebrahimi (Ed.). Nanocomposites - new trends and developments. IntechOpen, London, 2012.

[2] S Huang, X Zhu, S Sarkar and Y Zhao. Challenges and opportunities for supercapacitors. *APL Mater.* 2019; **7**, 100901.

[3] AZAL Shaqsi, K Sopian and A Al-Hinai. Review of energy storage services, applications, limitations, and benefits. *Energ. Rep.* 2020; **6**, 288-306.

[4] MIAA Maksoud, RA Fahim, AE Shalan, MA Elkodous, SO Olojede, AI Osman, C Farrell, AH Al-Muhtaseb, AS Awed, AH Ashour and DW Rooney. Advanced materials and technologies for supercapacitors used in energy conversion and storage: A review. *Environ. Chem. Lett.* 2021; **19**, 375-439.

[5] MB Tahir, M Abrar, A Tehseen, TI Awan, A Bashir and G Nabi. Chapter 11 - nanotechnology: The road ahead. *Chem. Nanometer.* 2020. https://doi.org/10.1016/B978-0-12-818908-5.00011-1.
[6] S Balasubramaniam, A Mohanty, SK Balasingam, SJ Kim and A Ramadoss. Comprehensive insight into the mechanism, material selection and performance evaluation of supercapatteries. *Nano Micro Lett.* 2020; **12**, 85.
[7] T Wilberforce, J Thompson and AG Olabi. Classification of energy storage materials. *Encycl. Smart Mater.* 2022; **2**, 8-14.
[8] J Liu, J Wang, C Xu, H Jiang, C Li, L Zhang, J Lin and ZX Shen. Advanced energy storage devices: Basic principles, analytical methods, and rational materials design. *Adv. Sci.* 2018; **5**, 1700322.
[9] A Numan, Y Zhan, M Khalid and M Hatamvand. Chapter three - introduction to supercapattery. *Adv. Supercapacitor Supercapattery* 2021. https://doi.org/10.1016/B978-0-12-819897-1.00008-2.
[10] PG Lebière, AP del Pino, C Logofatu and E György. Laser synthesis of NixZnyO/reduced graphene oxide/carbon nanotube electrodes for energy storage applications. *Appl. Surf. Sci.* 2021; **563**, 150234.
[11] H Li, Y Liu, S Lin, H Li, Z Wu, L Zhu, C Li, X Wang, X Zhu and Y Sun. Laser crystallized sandwich-like MXene/Fe_3O_4/MXene thin film electrodes for flexible supercapacitors. *J. Power Sourc.* 2021; **497**, 229882.
[12] R Wu, J Sun, X Ma, E Bao, X Du, C Xu and H Chen. Uniform $MgCo_2O_4$ porous nanoflakes and nanowires with superior electrochemical performance for asymmetric supercapacitors. *J. Alloy. Comp.* 2021; **884**, 161087.
[13] RL Naik, P Justin and TB Narsaiah. Size controlled hydrothermal synthesis and characterization of Nickel Metavanadate ($NiVO_3$) nanoparticles. *Int. J. Adv. Sci. Tech*. 2020; **29**, 10012-8.
[14] M Zheng, X Xiao, L Li, P Gu, X Dai, H Tang, Q Hu, H Xue and H Pang. Hierarchically nanostructured transition metal oxides for supercapacitors. *Sci. Chin. Mater.* 2018; **61**, 185-209.
[15] RL Naik, P Justin and TB Narsaiah. Controllable synthesis of cobalt vanadate nanostructure materials for direct methanol fuel cell applications. *In*: Proceedings of the International Conference on Advances in Chemical Engineering (AdChE), Uttarakhand, India. 2020.
[16] M Liu, B Su, Y Tang, X Jiang and A Yu. Recent advances in nanostructured vanadium oxides and composites for energy conversion. *Adv. Energ. Mater.* 2017; **7**, 1700885.
[17] S Beke. A review of the growth of V_2O_5 films from 1885 to 2010. *Thin Solid Films* 2011; **519**, 1761-71.
[18] R Liang, Y Du, P Xiao, J Cheng, S Yuan, Y Chen, J Yuan and J Chen. Transition metal oxide electrode materials for supercapacitors: A review of recent developments. *Nanomaterials* 2021; **11**, 1248.
[19] MAS Amulya, HP Nagaswarupa, MRA Kumar, CR Ravikumar and KB Kusuma. Enhanced photocatalytic and electrochemical properties of Cu doped $NiMnFe_2O_4$ nanoparticles synthesized via probe sonication method. *Appl. Surf. Sci.* 2020; **2**, 100038.
[20] X Wang, A Hu, C Meng, C Wu, S Yang and X Hong. Recent advance in Co_3O_4 and Co_3O_4-containing electrode materials for high-performance supercapacitors. *Molecules* 2020; **25**, 269.
[21] W Luo, JJ Gaumet and L Mai. Nanostructured layered vanadium oxide as cathode for high-performance sodium-ion batteries: A perspective. *MRS Comm.* 2017; **7**, 152-65.
[22] S Petnikota, R Chua, Y Zhou, E Edison and M Srinivasan. Amorphous vanadium oxide thin films as stable performing cathodes of lithium and sodium-ion batteries. *Nanoscale Res. Lett.* 2018; **13**, 363.
[23] O Monfort and P Petrisková. Binary and ternary vanadium oxides: General overview, physical properties, and photochemical processes for environmental applications. *Processes* 2021; **9**, 214.
[24] B Suganya, J Chandrasekaran, S Maruthamuthu, B Saravanakumar and E Vijayakumar. Hydrothermally synthesized zinc vanadate rods for electrochemical supercapacitance analysis in various aqueous electrolytes. *J. Inorg. Organomet. Polym. Meter.* 2020; **30**, 4510-9.
[25] J Yao, Y Li, RC Massé, E Uchaker and G Cao. Revitalized interest in vanadium pentoxide as cathode material for lithium-ion batteries and beyond. *Energ. Storage Mater.* 2018; **11**, 205259.
[26] K Cao, T Jin, L Yang and L Jiao. Recent progress in conversion reaction metal oxide anodes for Li-ion batteries. *Mater. Chem. Front.* 2017; **1**, 2213-42.
[27] X Zhang, C Jiang, J Liang and W Wu. Electrode materials and device architecture strategies for flexible supercapacitors in wearable energy storage. *J. Mater. Chem. A* 2021; **9**, 8099-128.
[28] LN Ramavathu, SR Harapanahalli, N Pernapati and BN Tumma. Synthesis and characterization of Nickel Metavanadate ($Ni_3V_2O_8$) - application as photocatalyst and supercapacitor. *Int. J. Nano Dimens.* 2021; **12**, 411-21.

[29] SE Arasi, P Devendran, R Ranjithkumar, S Arunpandiyan and A Arivarasan. Electrochemical property analysis of zinc vanadate nanostructure for efficient supercapacitors. *Mater. Sci. Semicond. Process.* 2020; **106**, 104785.

[30] CR Ravikumar, P Kotteeswaran, A Murugan, VB Raju, MS Santosh, HP Nagaswarupa, H Nagabhushana, SC Prashantha, MRA Kumar and K Gurushantha. Electrochemical studies of nano metal oxide reinforced nickel hydroxide materials for energy storage applications. *Mater. Today Proc.* 2017; **4**, 12205-14.

[31] M Wang, Y Shi and G Jiang. 3D hierarchical $Zn_3(OH)_2V_2O_7{\cdot}2H_2O$ and $Zn_3(VO_4)_2$ microspheres: Synthesis, characterization and photoluminescence. *Mater. Res. Bull.* 2012; **47**, 1823.

[32] H Guo, D Guo, Z Zheng, W Wen and J Chen. Hydrothermal synthesis and visible light photocatalytic activities of $Zn_3(VO_4)_2$ nanorods. *J. Mater. Res.* 2014; **29**, 2934-41.

[33] PA Putro, N Yudasari, I Isnaeni and A Maddu. Spectroscopy study of polyvinyl alcohol/carbon dots composite films. *Walailak J. Sci. Tech.* 2021; **18**, 9184.

[34] MAS Amulya, HP Nagaswarupa, MAR Kumar, CR Ravikumar and KB Kusuma. Sonochemical synthesis of $MnFe_2O_4$ nanoparticles and their electrochemical and photocatalytic properties. *J. Phys. Chem. Solid.* 2021; **148**, 109661.

[35] B Abebe, CR Ravikumar, EA Zereffa, AN Kumar and HCA Murthy. Photocatalytic and superior ascorbic acid sensor activities of PVA/Zn-Fe-Mn ternary oxide nanocomposite. *Inorg. Chem. Comm.* 2021; **123**, 108343.

[36] R Ranjitha, KN Meghana, VGD Kumar, AS Bhatt, BK Jayanna, CR Ravikumar, MS Santosh, H Madhyastha and K Sakai. Rapid photocatalytic degradation of cationic organic dyes using Li-doped Ni/NiO nanocomposites and their electrochemical performance. *New J. Chem.* 2021; **45**, 796-809.